



Nucleon-nucleon scattering up to next-to-next-to-leading order in manifestly Lorentz-invariant chiral effective field theory: peripheral phases

Xiu-Lei Ren 

*Institut für Kernphysik & Cluster of Excellence PRISMA⁺,
Johannes Gutenberg-Universität Mainz, D-55128 Mainz, Germany*

E. Epelbaum 

Institut für Theoretische Physik II, Ruhr-Universität Bochum, D-44780 Bochum, Germany

J. Gegelia 

*Institut für Theoretische Physik II, Ruhr-Universität Bochum, D-44780 Bochum, Germany and
High Energy Physics Institute, Tbilisi State University, 0186 Tbilisi, Georgia*

Abstract

We study the nucleon-nucleon interaction up to next-to-next-to-leading order using time-ordered perturbation theory in the framework of manifestly Lorentz-invariant chiral effective field theory. We present the two-pion exchange contribution at one-loop level, which is consistent with the corresponding non-relativistic expressions in the large-nucleon-mass limit. Using the Born series truncated at one-loop order, we calculate the phase shifts and mixing angles of the partial waves with the angular momentum $l \geq 2$. Comparing with the results of non-relativistic formulation, we find an improved description of the phase shifts for some D waves such as the 3D_3 one. For the other partial waves, both approaches show the globally similar results.

I. INTRODUCTION

Chiral effective field theory (ChEFT) for few-nucleon systems goes back to the seminal papers by Steven Weinberg, who extended chiral perturbation theory [1] to systems involving two and more nucleons [2, 3]. In the resulting ChEFT approach, the power counting rules are applied to the effective potentials defined as sums of contributions of few-nucleon-irreducible diagrams. The scattering amplitudes are then obtained by solving the Schrödinger equation or the corresponding integral equation in momentum space. For reviews of ChEFT in the few-body sector see Refs. [4–8].

In ChEFT one can only reliably calculate the effective potential for small momenta corresponding to its long-range part in the coordinate space. Loop integrals of scattering equations, on the other hand, involve integration over all momenta including the ultraviolet (UV) region. Naive extensions of the long-range parts of the chiral effective potentials to short distances result in singular potentials causing severe problems when solving equations. Such singular potentials generate deeply bound states that are absent in the underlying theory. The singular behavior of the chiral potentials at short distances therefore clearly represents an artifact of a naive extrapolation of the long-range potential to short distances. While the resulting arbitrariness should not influence physical observables if the renormalization is carried out properly by an appropriate treatment of the short range components encoded in contact interactions of the effective Lagrangian, in practice, carrying out correct quantum field theoretical renormalization in the few-body sector of ChEFT turned out to be a challenging problem. Conflicting points of view about this issue do not seem to converge to a consensus even after two decades of intense research. We refer interesting readers to Refs. [3, 9–41] for a collection of different points of view on this issue.

Aiming at an improved ultraviolet behavior of the effective potential, i.e. at its different UV extension, while keeping the same infrared (IR) behavior as in the standard non-relativistic formalism, a modified Weinberg’s approach to the nucleon-nucleon (NN) scattering problem has been proposed in Ref. [42]. This novel scheme employs time-ordered perturbation theory (TOPT) and relies on the manifestly Lorentz-invariant effective Lagrangian. It is important to emphasize that it was not thought as a replacement of the non-relativistic formalism but rather, being equivalent in the IR region, it results in a less divergent UV behavior leading to a perturbatively renormalizable modification of Weinberg’s approach. Based on this idea, a systematic framework for chiral nuclear forces with detailed diagrammatic rules of TOPT for particles with non-zero spin and interactions involving time derivatives has been worked out in Ref. [43]. These rules can be applied system-

atically at all orders in the loop expansion. Analogously to the non-relativistic approach, using the standard Weinberg power counting for diagrams contributing to NN scattering one has to take into account an infinite number of graphs already at leading order (LO). The infinite series of diagrams is resummed by defining the effective potential as a sum of all two-nucleon-irreducible TOPT diagrams and substituting into the Kadyshevsky integral equation [44]. The scattering amplitude can be calculated order-by-order using both a renormalizable approach, which relies on a perturbative treatment of corrections beyond LO and allows one to completely eliminate the UV cutoff, and a conventional scheme based on iterating a truncated potential to all orders while keeping the UV cutoff parameter of the order of the hard scale of the problem [25–27, 31–35]. In the latter case, the formulation based on the manifestly Lorentz-invariant effective Lagrangian is expected to permit a larger cutoff variation as compared to the non-relativistic approach thanks to the improved UV behavior.

To explicitly verify the above expectations it is necessary to go beyond LO in our manifestly Lorentz-invariant formulation.¹ Therefore, the main purpose of this paper is to derive the two-pion exchange (TPE) contributions up to next-to-next-to-leading order (NNLO), which are expected to describe the medium-range part of the NN interaction. Using the Born series truncated at one-loop order we calculate the phase shifts and mixing angles of the partial waves with orbital angular momentum $l \geq 2$ and compare our results with the empirical phase shifts as well as to the results of the non-relativistic ChEFT.

Our paper is organized as follows: in section II we specify the effective Lagrangian, give the diagrammatic rules of TOPT, and work out the details of the NN potential. Various checks of the obtained effective potential are performed and the phase shifts of peripheral partial waves are calculated and compared to analogous results in the non-relativistic formalism in section III. The results of our work are summarized in section IV.

II. TWO-PION-EXCHANGE CONTRIBUTIONS

In this section, we present the TPE contributions to the NN scattering amplitude at one-loop order. We start with the Lorentz-invariant effective chiral Lagrangian and briefly summarize the corresponding diagrammatic rules of TOPT obtained in Ref. [43]. Using the Weinberg power counting we identify all TPE diagrams contributing to the scattering amplitude up to NNLO.

¹ Different paths of calculating NN potential up to NNLO using relativistic ChEFT has been taken in Refs. [45–50].

Ultraviolet divergences and power-counting violating pieces of loop diagrams are removed by using the subtractive renormalization.

A. Effective chiral Lagrangian

The Lorentz-invariant effective chiral Lagrangian required for calculating one-loop contributions to the NN potential up to NNLO is given by

$$\mathcal{L}_{\text{eff}} = \mathcal{L}_{\pi\pi}^{(2)} + \mathcal{L}_{\pi N}^{(1)} + \mathcal{L}_{\pi N}^{(2)}, \quad (1)$$

where the superscripts denote the chiral orders, and [51–54]

$$\begin{aligned} \mathcal{L}_{\pi\pi}^{(2)} &= \frac{f_\pi^2}{4} \langle u_\mu u^\mu + \chi_+ \rangle, \\ \mathcal{L}_{\pi N}^{(1)} &= \bar{\Psi}_N \left\{ i \not{D} - m_N + \frac{g_A}{2} \not{u} \gamma^5 \right\} \Psi_N, \\ \mathcal{L}_{\pi N}^{(2)} &= \bar{\Psi}_N \left\{ c_1 \langle \chi_+ \rangle - \frac{c_2}{4m_N^2} \langle u^\mu u^\nu \rangle (D_\mu D_\nu + \text{h.c.}) + \frac{c_3}{2} \langle u^\mu u_\mu \rangle - \frac{c_4}{4} \gamma^\mu \gamma^\nu [u_\mu, u_\nu] \right\} \Psi_N. \end{aligned} \quad (2)$$

Leaving out the external sources, we have $u_\mu = i(u^\dagger \partial_\mu u - u \partial_\mu u^\dagger)$ and $\chi_+ = u^\dagger \chi u + u \chi u^\dagger$, with $u = \exp(i\Phi/2f_\pi)$ and $\chi = \text{diag}(M_\pi^2, M_\pi^2)$. The chiral covariant derivative acting on Ψ_N is given by $D_\mu \Psi_N = \partial_\mu \Psi_N + [\Gamma_\mu, \Psi_N]$ with $\Gamma_\mu = \frac{1}{2} (u^\dagger \partial_\mu u + u \partial_\mu u^\dagger)$. The pion and nucleon fields are collected in

$$\Phi = \begin{pmatrix} \pi^0 & \sqrt{2}\pi^+ \\ \sqrt{2}\pi^- & -\pi^0 \end{pmatrix}, \quad \Psi_N = \begin{pmatrix} p \\ n \end{pmatrix}. \quad (3)$$

The above specified effective Lagrangian depends on the following parameters: the pion decay constant f_π , the axial vector coupling g_A , the pion mass M_π , the nucleon mass m_N and the four low-energy constants (LECs) c_1, c_2, c_3, c_4 , introduced in the πN Lagrangian of the second order, $\mathcal{L}_{\pi N}^{(2)}$. Numerical values of these parameters will be specified in the next section.

B. Diagrammatic rules of TOPT

To derive the NNLO chiral potential, we apply the diagrammatic rules of TOPT to the manifestly Lorentz-invariant effective Lagrangian. These rules were obtained in Ref. [43] and are briefly summarized below.

For the elastic NN scattering process, $N(p_1) + N(p_2) \rightarrow N(p_3) + N(p_4)$, the S matrix can be written as

$$S = 1 - (2\pi)^4 i T \delta^4(p_3 + p_4 - p_1 - p_2) \prod_{i=1}^4 (2\pi)^{-3/2} \left(\frac{m_N}{\omega_{p_i}} \right)^{1/2}, \quad (4)$$

where the four-momenta of the initial and final states are $p_1^\mu = (\omega_p, \mathbf{p})$, $p_2^\mu = (\omega_p, -\mathbf{p})$, $p_3^\mu = (\omega_{p'}, \mathbf{p}')$, and $p_4^\mu = (\omega_{p'}, -\mathbf{p}')$. Here \mathbf{p} and \mathbf{p}' are the three-momenta of the incoming and outgoing nucleons in the center-of-mass frame, respectively, and the nucleon energy is defined as $\omega_l := \sqrt{\mathbf{l}^2 + m_N^2}$. The (on-shell) scattering amplitude T can be given as a sum of an infinite number of time-ordered diagrams. Contribution of each diagram is evaluated via the following diagrammatic rules:

- Draw all possible time-ordered diagrams contributing to NN scattering at a given order in the loop expansion and having the same combination of coupling constants;
- Assign to each incoming (outgoing) external nucleon line with momentum p_i (p'_i) Dirac spinor $u(p_i)$ ($\bar{u}(p'_i)$);
- Assign to each internal nucleon line a factor

$$\frac{m_N}{\omega_{p_i}} \sum u(p_i) \bar{u}(p_i), \quad (5)$$

where the sum is carried out over polarizations;

- Assign to each internal anti-nucleon-line a factor

$$\frac{m_N}{\omega_{p_i}} \sum u(p_i) \bar{u}(p_i) - \gamma_0, \quad (6)$$

where γ_0 is the Dirac gamma matrix;

- Each internal pion line gives a factor

$$\frac{1}{2\varepsilon_{p_\pi}} \quad (7)$$

with the pion four-momentum p_π and the pion energy defined as $\varepsilon_l := \sqrt{\mathbf{l}^2 + M_\pi^2}$;

- Each intermediate state gives an energy denominator

$$\frac{1}{E - \sum_i \omega_{p_i} - \sum_j \varepsilon_{p_j} + i\epsilon}, \quad (8)$$

where E is the total energy of the NN system and the indices i, j label the internal nucleon/pion lines in the intermediate state;

- Each interaction vertex is obtained using the standard Feynman rules, special care needs to be taken of the zeroth components of momenta appearing in vertices. Details can be found in Ref. [43];
- While each one-loop diagram with internal momentum k contains a three-dimensional integration

$$\int \frac{d^3 k}{(2\pi)^3} . \quad (9)$$

C. The NN T -matrix at one loop order

Here we present the results for the NN T -matrix at one-loop order. It contains two pieces: the TPE potential and the once-iterated one-pion-exchange (OPE) potential. Notice that the one-loop corrections to the OPE potential are included by expressing the OPE potential in terms of physical coupling constants.

1. Two-pion exchange potential

We apply the standard Weinberg power counting to derive the chiral potential [2, 3]. The TPE potential at one-loop order contains two parts: $V_{2\pi}^{(\nu=2)}$ and $V_{2\pi}^{(\nu=3)}$, where ν indicates chiral orders of time-ordered diagrams,

$$\nu = 2l + \sum_i V_i \left(d_i + \frac{n_i}{2} - 2 \right) , \quad (10)$$

where l is the number of loops, V_i is the number of vertices of type i , d_i is the number of derivatives acting on pion fields and/or spatial components of derivatives acting on nucleon fields, or pion-mass insertions, and n_i denotes the number of nucleon fields involved in vertex i . The sum in the above equation runs over all vertices contained in the diagram.

At second order ($\nu = 2$), the two-nucleon irreducible time-ordered diagrams contributing to the TPE potential are shown in Fig. 1,

$$V_{2\pi}^{(\nu=2)} = V_F^{(2)} + V_{T+\bar{T}}^{(2)} + V_B^{(2)} + V_{\bar{B}}^{(2)} . \quad (11)$$

Using the TOPT rules and keeping only the LO terms in the expansion of the Dirac spinors in small momenta,

$$u = u_0 + u_1 + \cdots , \quad \bar{u} = \bar{u}_0 + \bar{u}_1 + \cdots , \quad (12)$$

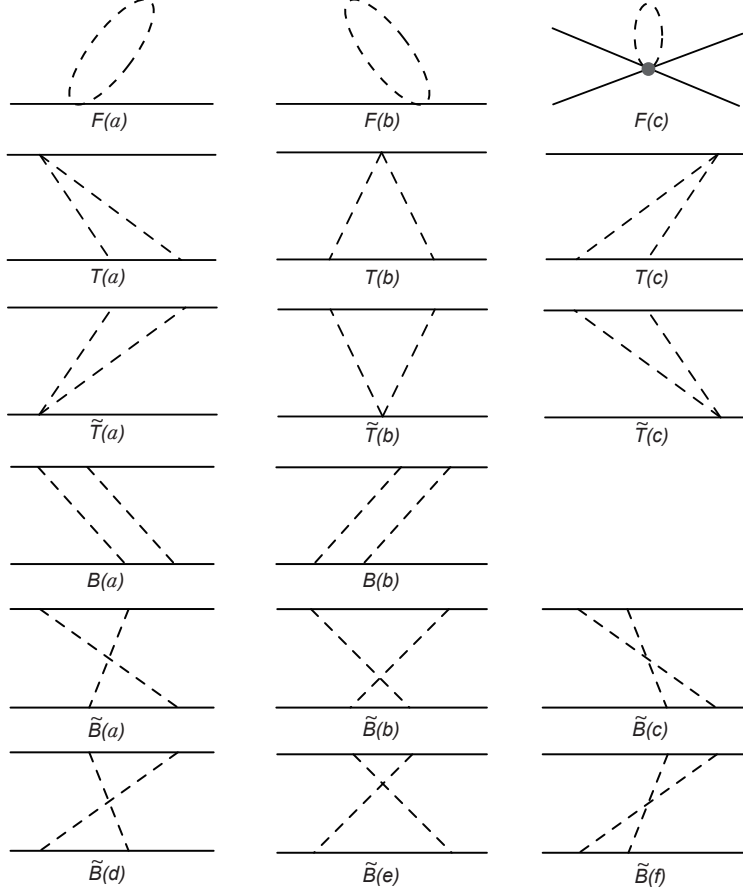


Figure 1. Time-ordered diagrams contributing to the TPE potential at NLO. Solid and dashed lines correspond to nucleons and pions, respectively. The pion-nucleon vertices are from $\mathcal{L}_{\pi N}^{(1)}$.

where $u_0 = P_+ u(p)$ and $\bar{u}_0 = \bar{u}(p) P_+$ with $P_+ \equiv (1 + \not{v})/2$ and $v = (1, 0, 0, 0)$, we obtain the following expressions:

- Contribution of the football diagrams [the sum of diagrams $F(a)$ - $F(c)$ in Fig. 1]

$$V_F^{(2)} = \frac{\boldsymbol{\tau}_1 \cdot \boldsymbol{\tau}_2}{16f_\pi^4} \int \frac{d^3k}{(2\pi)^3} \frac{(\varepsilon_k + \varepsilon_{k+q})(\omega_p + \omega_{p'}) + 4\varepsilon_k \varepsilon_{k+q} - E(\varepsilon_k + \varepsilon_{k+q})}{2\varepsilon_k \varepsilon_{k+q} (\varepsilon_k + \varepsilon_{k+q} + \omega_p + \omega_{p'} - E)}, \quad (13)$$

where $\boldsymbol{\tau}_i$ denote the isospin Pauli matrices of nucleon i , E is the total energy of the two-nucleon system, and the momentum transfer is given by $\mathbf{q} = \mathbf{p}' - \mathbf{p}$. Notice that the third diagram, $F(c)$, is due to the zeroth component of momentum appearing in the vertex corresponding to the Weinberg-Tomozawa interaction [3, 55].

- Contribution of triangle diagrams [the sum of diagrams $T(a) - T(c)$ and $\tilde{T}(a) - \tilde{T}(c)$ in

Fig. 1]

$$V_{T+\tilde{T}}^{(2)} = \frac{4m_N g_A^2 \boldsymbol{\tau}_1 \cdot \boldsymbol{\tau}_2}{128 f_\pi^4} \int \frac{d^3 k}{(2\pi)^3} \left[(\mathbf{k}^2 + (\mathbf{p}' - \mathbf{p}) \cdot \mathbf{k}) + \frac{i(\boldsymbol{\sigma}_1 + \boldsymbol{\sigma}_2) \cdot \mathbf{n}}{2} (a + b) \right] \quad (14)$$

$$\times \left[\frac{\varepsilon_{k+q} - \varepsilon_k}{\varepsilon_k \varepsilon_{k+q} \omega_{p-k}} \left(\frac{1}{D_{T_a}} + \frac{1}{D_{\tilde{T}_a}} - \frac{1}{D_{T_c}} - \frac{1}{D_{\tilde{T}_c}} \right) + \frac{\varepsilon_k + \varepsilon_{k+q}}{\varepsilon_k \varepsilon_{k+q} \omega_{p-k}} \left(\frac{1}{D_{T_b}} + \frac{1}{D_{\tilde{T}_b}} \right) \right],$$

where $\boldsymbol{\sigma}_i$ refer to the spin Pauli matrices of the nucleon i , $\mathbf{n} = \mathbf{p} \times \mathbf{p}'$, and the denominators corresponding to intermediate states are given by:

$$\begin{aligned} D_{T_a} &= (E - \omega_{k-p} - \varepsilon_{k+q} - \omega_{p'}) (E - \varepsilon_{k+q} - \varepsilon_k - \omega_p - \omega_{p'}), \\ D_{T_b} &= (E - \omega_{k-p} - \varepsilon_k - \omega_p) (E - \omega_{k-p} - \varepsilon_{k+q} - \omega_{p'}), \\ D_{T_c} &= (E - \omega_{k-p} - \varepsilon_k - \omega_p) (E - \varepsilon_{k+q} - \varepsilon_k - \omega_p - \omega_{p'}), \\ D_{\tilde{T}_a} &= (E - \omega_{k-p} - \varepsilon_{k+q} - \omega_{p'}) (E - \varepsilon_{k+q} - \varepsilon_k - \omega_p - \omega_{p'}), \\ D_{\tilde{T}_b} &= (E - \omega_{k-p} - \varepsilon_k - \omega_p) (E - \omega_{k-p} - \varepsilon_{k+q} - \omega_{p'}), \\ D_{\tilde{T}_c} &= (E - \omega_{k-p} - \varepsilon_k - \omega_p) (E - \varepsilon_{k+q} - \varepsilon_k - \omega_p - \omega_{p'}). \end{aligned} \quad (15)$$

The parameters a and b in Eq. (15) stand for the coefficients of the decomposition $\mathbf{k} = a\mathbf{p} + b\mathbf{p}' + c(\mathbf{p}' \times \mathbf{p})$, where

$$a = \frac{\mathbf{p}' \cdot \mathbf{p} \mathbf{p}' \cdot \mathbf{k} - \mathbf{p}'^2 \mathbf{p} \cdot \mathbf{k}}{(\mathbf{p}' \cdot \mathbf{p})^2 - \mathbf{p}'^2 \mathbf{p}^2}, \quad b = \frac{\mathbf{p}' \cdot \mathbf{p} \mathbf{p} \cdot \mathbf{k} - \mathbf{p}^2 \mathbf{p}' \cdot \mathbf{k}}{(\mathbf{p}' \cdot \mathbf{p})^2 - \mathbf{p}^2 \mathbf{p}'^2}, \quad c = \frac{(\mathbf{p}' \times \mathbf{p}) \cdot \mathbf{k}}{|\mathbf{p}' \times \mathbf{p}|^2}. \quad (16)$$

- Contribution of planar box diagrams [the sum of diagrams $B(a)$ and $B(b)$ in Fig. 1]

$$V_B^{(2)} = \frac{m_N^2 g_A^4 (3 - 2 \boldsymbol{\tau}_1 \cdot \boldsymbol{\tau}_2)}{64 f_\pi^4} \int \frac{d^3 k}{(2\pi)^3} \left[X_1 + X_2 \boldsymbol{\sigma}_1 \cdot \boldsymbol{\sigma}_2 + X_3 \frac{i(\boldsymbol{\sigma}_1 + \boldsymbol{\sigma}_2) \cdot \mathbf{n}}{2} \right. \quad (17)$$

$$\left. + X_4 (\boldsymbol{\sigma}_1 \cdot \mathbf{n}) (\boldsymbol{\sigma}_2 \cdot \mathbf{n}) + X_5 (\boldsymbol{\sigma}_1 \cdot \mathbf{q}) (\boldsymbol{\sigma}_2 \cdot \mathbf{q}) \right] \frac{1}{\varepsilon_k \varepsilon_{k+q} \omega_{k-p}^2} \left(\frac{1}{D_{B_a}} + \frac{1}{D_{B_b}} \right),$$

where the denominators corresponding to the intermediate states are given by:

$$\begin{aligned} D_{B_a} &= (E - \omega_{k-p} - \varepsilon_k - \omega_p) (E - \varepsilon_{k+q} - \varepsilon_k - \omega_p - \omega_{p'}) (E - \omega_{k-p} - \varepsilon_{k+q} - \omega_{p'}), \\ D_{B_b} &= (E - \omega_{k-p} - \varepsilon_k - \omega_p) (E - \varepsilon_{k+q} - \varepsilon_k - \omega_p - \omega_{p'}) (E - \omega_{k-p} - \varepsilon_{k+q} - \omega_{p'}). \end{aligned} \quad (18)$$

The coefficients X_i in Eq. (17) are the following functions of a, b and c :

$$\begin{aligned} X_1 &= [\mathbf{k}^2 + \mathbf{q} \cdot \mathbf{k}]^2, \quad X_2 = -c^2 \mathbf{q}^2 [\mathbf{P}^2 \mathbf{q}^2 - (\mathbf{q} \cdot \mathbf{P})^2], \\ X_3 &= -2(a + b) (\mathbf{k}^2 + (\mathbf{p}' - \mathbf{p}) \cdot \mathbf{k}), \quad X_4 = -(a + b)^2 + c^2 \mathbf{q}^2, \\ X_5 &= c^2 [\mathbf{P}^2 \mathbf{q}^2 - (\mathbf{q} \cdot \mathbf{P})^2], \end{aligned} \quad (19)$$

with $\mathbf{P} = 1/2(\mathbf{p} + \mathbf{p}')$.

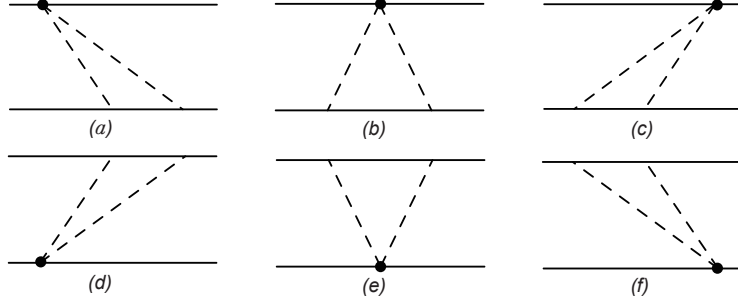


Figure 2. Time-ordered diagrams contributing to the TPE potential at NNLO. Solid and dashed lines correspond to nucleons and pions, respectively. The filled circles denote the vertices from $\mathcal{L}_{\pi N}^{(2)}$.

- Contribution of crossed box diagrams [the sum of diagrams $\tilde{B}(a) - \tilde{B}(f)$ in Fig. 1]

$$\begin{aligned}
 V_{\tilde{B}}^{(2)} = & \frac{m_N^2 g_A^4 (3 + 2\boldsymbol{\tau}_1 \cdot \boldsymbol{\tau}_2)}{64 f_\pi^4} \int \frac{d^3 k}{(2\pi)^3} [X_1 - X_2 \boldsymbol{\sigma}_1 \cdot \boldsymbol{\sigma}_2 - X_4 (\boldsymbol{\sigma}_1 \cdot \mathbf{n}) (\boldsymbol{\sigma}_2 \cdot \mathbf{n}) \\
 & - X_5 (\boldsymbol{\sigma}_1 \cdot \mathbf{q}) (\boldsymbol{\sigma}_2 \cdot \mathbf{q})] \frac{1}{\varepsilon_k \varepsilon_{k+q} \omega_{p-k} \omega_{p'+k}} \\
 & \times \left(\frac{1}{D_{\tilde{B}_a}} + \frac{1}{D_{\tilde{B}_b}} + \frac{1}{D_{\tilde{B}_c}} + \frac{1}{D_{\tilde{B}_d}} + \frac{1}{D_{\tilde{B}_e}} + \frac{1}{D_{\tilde{B}_f}} \right),
 \end{aligned} \tag{20}$$

where the denominators corresponding to intermediate states are given by:

$$\begin{aligned}
 D_{\tilde{B}_a} &= (E - \omega_{k-p} - \varepsilon_k - \omega_p) (E - \omega_{k+p'} - \varepsilon_k - \omega_{p'}) (E - \omega_{k-p} - \omega_{k+p'} - \varepsilon_{k+q} - \varepsilon_k), \\
 D_{\tilde{B}_b} &= (E - \omega_{k-p} - \varepsilon_k - \omega_p) (E - \omega_{k-p} - \varepsilon_{k+q} - \omega_{p'}) (E - \omega_{k-p} - \omega_{k+p'} - \varepsilon_{k+q} - \varepsilon_k), \\
 D_{\tilde{B}_c} &= (E - \omega_{k-p} - \varepsilon_k - \omega_p) (E - \omega_{k+p'} - \varepsilon_k - \omega_{p'}) (E - \varepsilon_{k+q} - \varepsilon_k - \omega_p - \omega_{p'}), \\
 D_{\tilde{B}_d} &= (E - \omega_{k+p'} - \varepsilon_{k+q} - \omega_p) (E - \omega_{k-p} - \varepsilon_{k+q} - \omega_{p'}) (E - \omega_{k-p} - \omega_{k+p'} - \varepsilon_{k+q} - \varepsilon_k), \\
 D_{\tilde{B}_e} &= (E - \omega_{k+p'} - \varepsilon_{k+q} - \omega_p) (E - \omega_{k+p'} - \varepsilon_k - \omega_{p'}) (E - \omega_{k-p} - \omega_{k+p'} - \varepsilon_{k+q} - \varepsilon_k), \\
 D_{\tilde{B}_f} &= (E - \omega_{k+p'} - \varepsilon_{k+q} - \omega_p) (E - \omega_{k-p} - \varepsilon_{k+q} - \omega_{p'}) (E - \varepsilon_{k+q} - \varepsilon_k - \omega_p - \omega_{p'}).
 \end{aligned} \tag{21}$$

The diagrams giving non-vanishing contributions to the TPE potential at third order ($\nu = 3$, NNLO) in our calculations are shown in Fig. 2, where the football diagrams do not contribute since we keep only the LO terms in the expansion of the Dirac spinors. Then, using the TOPT rules we

obtain the following contribution

$$\begin{aligned}
V_{2\pi}^{(\nu=3)} = & \frac{3m_N g_A^2}{16f_\pi^4} \int \frac{d^3k}{(2\pi)^3} \left[(\mathbf{k}^2 + (\mathbf{p}' - \mathbf{p}) \cdot \mathbf{k}) - (a+b) \frac{i(\boldsymbol{\sigma}_1 + \boldsymbol{\sigma}_2) \cdot \mathbf{n}}{2} \right] \frac{1}{\varepsilon_k \varepsilon_{k+q} \omega_{p-k}} \\
& \times \left\{ \left[4c_1 M_\pi^2 - \frac{c_2}{m_N^2} \left(\mathbf{p} \cdot \mathbf{k} \mathbf{p} \cdot (\mathbf{k} + \mathbf{q}) + \mathbf{p}' \cdot \mathbf{k} \mathbf{p}' \cdot (\mathbf{k} + \mathbf{q}) \right) + 2c_3 \mathbf{k} \cdot (\mathbf{k} + \mathbf{q}) \right] \right. \\
& \times \left(\frac{1}{D_a} + \frac{1}{D_b} + \frac{1}{D_c} + \frac{1}{D_d} + \frac{1}{D_e} + \frac{1}{D_f} \right) \\
& + \left[\frac{c_2}{m_N^2} \varepsilon_k \varepsilon_{k+q} (\omega_p + \omega_{p'}) + 2c_3 \varepsilon_k \varepsilon_{k+q} \right] \left(\frac{1}{D_a} - \frac{1}{D_b} + \frac{1}{D_c} + \frac{1}{D_d} - \frac{1}{D_e} + \frac{1}{D_f} \right) \\
& + \left[\frac{c_2}{m_N^2} \varepsilon_k (\omega_p \mathbf{p} \cdot (\mathbf{k} + \mathbf{q}) + \omega_{p'} \mathbf{p}' \cdot (\mathbf{k} + \mathbf{q})) \right] \left(\frac{1}{D_a} - \frac{1}{D_b} - \frac{1}{D_c} + \frac{1}{D_d} - \frac{1}{D_e} - \frac{1}{D_f} \right) \\
& \left. - \left[\frac{c_2}{m_N^2} \varepsilon_{k+q} (\omega_p \mathbf{p} \cdot \mathbf{k} + \omega_{p'} \mathbf{p}' \cdot \mathbf{k}) \right] \left(\frac{1}{D_a} + \frac{1}{D_b} - \frac{1}{D_c} + \frac{1}{D_d} + \frac{1}{D_e} - \frac{1}{D_f} \right) \right\} \\
& + \frac{c_4 m_N g_A^2 \boldsymbol{\tau}_1 \cdot \boldsymbol{\tau}_2}{8f_\pi^4} \int \frac{d^3k}{(2\pi)^3} \left[X_2 \boldsymbol{\sigma}_1 \cdot \boldsymbol{\sigma}_2 + \frac{X_3}{2} \frac{i(\boldsymbol{\sigma}_1 + \boldsymbol{\sigma}_2) \cdot \mathbf{n}}{2} + X_4 (\boldsymbol{\sigma}_1 \cdot \mathbf{n}) (\boldsymbol{\sigma}_2 \cdot \mathbf{n}) \right. \\
& \left. + X_5 (\boldsymbol{\sigma}_1 \cdot \mathbf{q}) (\boldsymbol{\sigma}_2 \cdot \mathbf{q}) \right] \frac{1}{\varepsilon_{k+q} \omega_{p-k}} \left(\frac{1}{D_a} + \frac{1}{D_b} + \frac{1}{D_c} + \frac{1}{D_d} + \frac{1}{D_e} + \frac{1}{D_f} \right), \tag{22}
\end{aligned}$$

where the denominators corresponding to the intermediate states in diagrams of Figs. 2 (a)-(f) are the same as the ones given in Eq. (15), i.e.

$$D_a = D_{T_a}, \quad D_b = D_{T_b}, \quad D_c = D_{T_c}, \quad D_d = D_{\tilde{T}_a}, \quad D_e = D_{\tilde{T}_b}, \quad D_f = D_{\tilde{T}_c}. \tag{23}$$

To renormalize the one-loop diagrams we apply subtractive renormalization by expanding the integrands in powers of the external momenta and the pion mass and subtracting those contributions which lead to divergent and power counting violating contributions in the removed cutoff limit. We checked explicitly that all these subtraction terms are indeed cancelled by appropriate local counter terms of the NN contact interaction Lagrangian. The renormalized contributions of the TOPT diagrams are calculated numerically.

2. Once-iterated one-pion exchange

Using the previous diagrammatic rules of TOPT, we obtain the OPE potential

$$V_{\text{OPE}} = -\frac{g_A^2}{4f_\pi^2} \boldsymbol{\tau}_1 \cdot \boldsymbol{\tau}_2 \frac{1}{\varepsilon_q} \frac{(\bar{u}_3 \gamma^\mu \gamma_5 q_\mu u_1) (\bar{u}_4 \gamma^\nu \gamma_5 q_\nu u_2)}{\omega_p + \omega_{p'} + \varepsilon_q - E - i\epsilon}. \tag{24}$$

Apparently, when dealing with the once-iterated OPE potential

$$V_{\text{OPE}} G V_{\text{OPE}} = \int \frac{d^3k}{(2\pi)^3} \frac{m_N^2}{\mathbf{k}^2 + m_N^2} \frac{V_{\text{OPE}}(p', k) V_{\text{OPE}}(k, p)}{E - 2\omega_k + i\epsilon}, \quad (25)$$

where the energy denominator is just the two-nucleon Green function of the Kadyshevsky equation, one encounters the poles in the denominators of the half-off-shell OPE potentials $V_{\text{OPE}}(p', k)$ and $V_{\text{OPE}}(k, p)$. To avoid this technical complication it is convenient to eliminate the energy-dependence of the OPE potential $V_{\text{OPE}}(p, p')$ by performing an expansion in powers of $E - \omega_p - \omega_{p'}$, and obtain, up to the accuracy of our calculation, an equivalent energy-independent potential $V_{\not{E}} = V_{\text{OPE}, \not{E}}^{(0)} + V_{2\pi, \not{E}}^{(2)}$, which satisfies

$$V_{\text{OPE}} + V_{\text{OPE}} G V_{\text{OPE}} = V_{\text{OPE}, \not{E}}^{(0)} + V_{2\pi, \not{E}}^{(2)} + V_{\text{OPE}, \not{E}}^{(0)} G V_{\text{OPE}, \not{E}} + \mathcal{O}(\nu = 4), \quad (26)$$

where the energy-independent OPE potential is given by

$$V_{\text{OPE}, \not{E}}^{(0)} = -\frac{g_A^2 \boldsymbol{\tau}_1 \cdot \boldsymbol{\tau}_2}{4f_\pi^2} \frac{1}{\varepsilon_q^2} (\bar{u}_3 \gamma_\mu \gamma_5 q^\mu u_1) (\bar{u}_4 \gamma_\nu \gamma_5 q^\nu u_2), \quad (27)$$

and, for simplicity, we keep the full form of Dirac spinors of the nucleon, which is equivalent to including also higher order contributions of the OPE potential. The second term $V_{2\pi, \not{E}}^{(2)}$ is written as

$$V_{2\pi, \not{E}}^{(2)} = \frac{1}{2} \left(\frac{g_A^2}{4f_\pi^2} \right)^2 (3 - \boldsymbol{\tau}_1 \cdot \boldsymbol{\tau}_2) \int \frac{d^3k}{(2\pi)^3} \frac{m_N^2}{\mathbf{k}^2 + m_N^2} \frac{\varepsilon_{p'-k} + \varepsilon_{p-k}}{\varepsilon_{p'-k}^3 \varepsilon_{p-k}^3} \times [\boldsymbol{\sigma}_1 \cdot (\mathbf{p}' - \mathbf{k}) \boldsymbol{\sigma}_1 \cdot (\mathbf{k} - \mathbf{p})] [\boldsymbol{\sigma}_2 \cdot (\mathbf{p}' - \mathbf{k}) \boldsymbol{\sigma}_2 \cdot (\mathbf{k} - \mathbf{p})], \quad (28)$$

where we keep only the LO terms in the expansion of the Dirac spinors, similarly to the treatment of TPE potential in the last subsection. Notice that the $V_{2\pi, \not{E}}^{(2)}$ is obtained by cancelling the Kadyshevsky denominator and is the part of the TPE potential at NLO, which has the same spin structure as the planar box diagram of the same order.

According to the above discussion, the once-iterated OPE potential leads to

$$V_{2\pi, it}(p', p) = V_{\text{OPE}, \not{E}}^{(0)} G V_{\text{OPE}, \not{E}}^{(0)} = \int \frac{d^3k}{(2\pi)^3} \frac{m_N^2}{\mathbf{k}^2 + m_N^2} \frac{V_{\text{OPE}, \not{E}}^{(0)}(p', k) V_{\text{OPE}, \not{E}}^{(0)}(k, p)}{E - 2\omega_k + i\epsilon}. \quad (29)$$

We found that $V_{\text{OPE}}^{(0)}(p', p)$ has a milder ultraviolet behavior compared to its non-relativistic analogue. In particular for fixed p' and large p we have $V_{\text{OPE}}^{(0)} \sim 1/p$. The benefit comes to the once-iterated OPE potential, which is UV convergent for all partial waves. This allows us to directly calculate the integral by using the standard Gauss-Legendre quadratures. While the non-relativistic counterpart of the once-iterated OPE potential is linearly divergent, one can use the dimensional regularization to obtain a closed finite form, as done in Ref. [56].

3. NN T -matrix and phase shifts

Finally, we obtain the T -matrix of NN scattering at one-loop order in the Born expansion

$$\begin{aligned} T(p', p) &= V_{\text{OPE}, \cancel{E}}^{(0)}(p', p) + V_{2\pi, \cancel{E}}^{(2)}(p', p) + V_{2\pi, irr}^{(2)}(p', p) + V_{2\pi, irr}^{(3)}(p', p) + V_{2\pi, it}(p', p) \\ &= V_{\text{OPE}, \cancel{E}}^{(0)}(p', p) + V_{2\pi, irr}(p', p) + V_{2\pi, it}(p', p), \end{aligned}$$

where $V_{2\pi, irr}$ refers to the NN potential as the sum of all two-nucleon irreducible TPE contributions up to NNLO: $V_{2\pi, irr} = V_{2\pi, \cancel{E}}^{(2)} + V_{2\pi, irr}^{(2)} + V_{2\pi, irr}^{(3)}$.

We follow the steps given in Ref. [57] and perform the partial wave decomposition of the NN T -matrix to express it in the standard lsj representation. Then, the phase shifts and mixing angles can be perturbatively calculated via [56, 58]

$$\begin{aligned} \delta_l^{sj} &= -\frac{p m_N^2}{16\pi^2 \sqrt{p^2 + m_N^2}} \text{Re} \langle lsj | T | lsj \rangle, \\ \epsilon_j &= \frac{p m_N^2}{16\pi^2 \sqrt{p^2 + m_N^2}} \text{Re} \langle j-1, 1, j | T | j+1, 1, j \rangle, \end{aligned} \tag{30}$$

where $p \equiv |\mathbf{p}|$.

III. PERIPHERAL PHASE SHIFTS

In this section we calculate the NN phase shifts and mixing angles for partial waves with the angular momenta $l \geq 2$ and $j \geq 2$, and compare them with the corresponding results of the non-relativistic approach. We start by first performing the consistency checks of our results for the TPE potential $V_{2\pi, irr}$ up to NNLO and the once-iterated OPE, $V_{2\pi, it}$, by taking the large m_N limit.

The values of parameters used in the following calculations are as follows: the average pion and nucleon masses $M_\pi = 138$ MeV and $m_N = 938.918$ MeV, the pion decay constant $f_\pi = 92.4$ MeV is fixed to its physical value; the axial coupling g_A fixed as 1.267 for LO calculation, and changed to 1.29 to account for the Goldberger-Treiman discrepancy at NLO and NNLO. For our NNLO calculations, we also need to specify the numerical values of the LECs c_1 , c_2 , c_3 , and c_4 . We take $c_1 = -0.74$ GeV⁻¹, $c_2 = 1.81$ GeV⁻¹, $c_3 = -3.61$ GeV⁻¹, and $c_4 = 2.17$ GeV⁻¹ obtained from the order- Q^2 matching to the πN subthreshold parameters, determined by the Roy-Steiner analysis of πN scattering [59], using the covariant formulation of ChEFT [60]. We use the same values for parameters to obtain the NNLO results of the non-relativistic ChEFT.

A. Consistency checks of the two-pion exchange contributions

For D , F and higher partial waves, there are no contact-interaction contributions to the potential at NLO and NNLO. Thus, our irreducible TPE potential obtained using the subtractive renormalization and the non-relativistic TPE potential calculated using the dimensional regularization should give the same results when the nucleon mass m_N is taken to infinity. This can be verified numerically with good accuracy by calculating the phase shifts in both approaches for large values of the nucleon mass.

In Fig. 3 we present some typical phase shifts of D and F waves given by the irreducible TPE diagrams in our scheme for the physical nucleon mass m_N^{Phys} and for a large nucleon mass $m_N = 1000 m_N^{\text{Phys}}$. Our results are consistent with the ones of the non-relativistic TPE potential. Notice that our TPE contributions up to NNLO for the physical value of the nucleon mass are smaller in magnitude than their non-relativistic analogues, particularly for the 3D_3 partial wave.

Furthermore, we also present the consistency check of the once-iterated OPE contribution in Fig. 4, where the phase shifts of several partial waves receiving sizable contributions from $V_{2\pi,it}$ are shown. To check the reliability of our numerical evaluation, we take m_N in $V_{2\pi,it}$ to infinity and indeed reproduce the non-relativistic results obtained using the analytic expressions of the once-iterated OPE potential, as specified by Eqs. (31)-(34) in Ref. [56]. Notice that the relativistic correction factor $m_N/\sqrt{m_N^2 + p^2}$ included in Eq. (24) of Ref. [56] needs to be removed for the purposes of our comparison. We can see that for the physical nucleon mass the phase shifts obtained using our $V_{2\pi,it}$ are smaller than the ones of the non-relativistic case, particularly for the 3D_3 partial

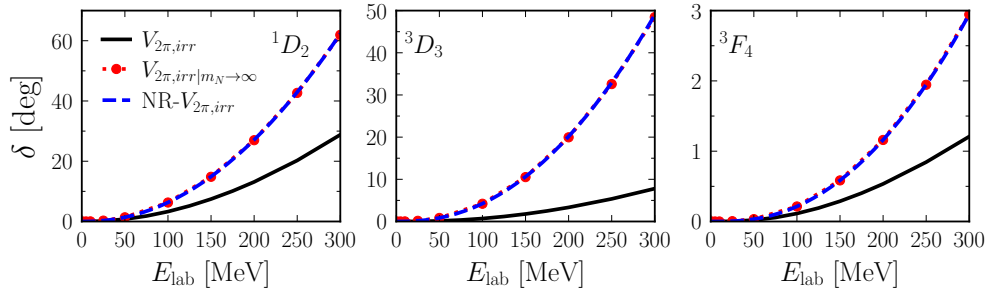


Figure 3. The phase shifts of 1D_2 , 3D_3 and 3F_4 partial waves from the TPE potential up to NNLO. The black solid lines denote our results with the physical nucleon mass, the red dotted lines are generated by taking m_N in TPE potential to infinity (numerically we take $m_N = 1000 m_N^{\text{Phys}}$). The blue dashed lines are the results of non-relativistic TPE potential.

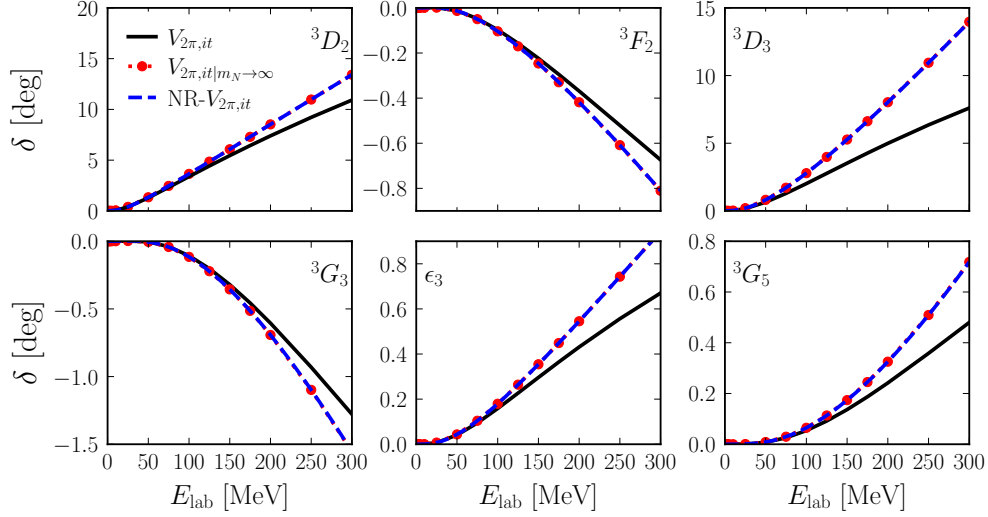


Figure 4. Partial wave phase shifts corresponding to the once-iterated OPE potential. The black solid lines denote our results with the physical nucleon mass, the red dotted lines are generated by taking m_N in $V_{2\pi,it}$ to infinity (numerically we take $m_N = 1000 m_N^{\text{Phys}}$). The blue dashed lines are the results of non-relativistic once-iterated OPE potential.

wave. That is because the once-iterated OPE potential is slightly less attractive/repulsive than its non-relativistic counterpart.

B. Peripheral phase shifts

Below we present our results for the partial wave phase shifts for $l \geq 2$ and $j \geq 2$ using our chiral potential up to NNLO.

1. D-waves

Our results for the D-wave phase shifts and the mixing angle ϵ_2 are presented in Fig. 5. The LO result (corresponding to the pure OPE potential), shown by the green dot-dashed curves, provides the major contributions to 3D_2 and ϵ_2 but is too weak in the 1D_2 channel and gives the opposite trend in comparison with the empirical phase shifts for the 3D_3 partial wave. Including the NLO correction obtained using the subtractive renormalization gives the correct direction of improvement for all D-wave phase shifts, as shown by the blue dashed lines. However its contribution is relatively small, which is (partly) due to the strong cancelation between the leading TPE potential and the

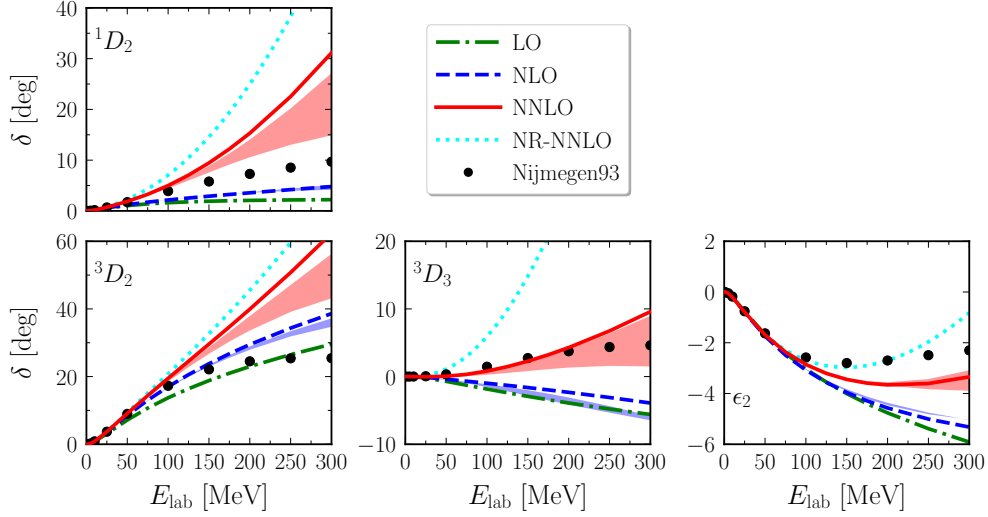


Figure 5. D -wave neutron-proton phase shifts and the mixing angle ϵ_2 for laboratory energies below 300 MeV. The green dot-dashed curve is the LO result (which corresponds to the pure OPE), the blue dashed and red solid lines denote the NLO and NNLO results, respectively. The non-relativistic results at NNLO are shown as the cyan dotted lines. The filled circles represent the results of the Nijmegen partial wave analysis [61]. The light-blue and red bands correspond to the NLO and NNLO potentials with the loop integrals in the TPE diagrams regulated using the cutoff $\Lambda = 500 - 800$ MeV.

once-iterated OPE. For example, the contributions of $V_{2\pi, it}$ to the 3D_2 and 3D_3 partial waves are quite large, as seen in Fig. 4, but adding them to the contributions of the strongly repulsive TPE potential results in small attractive contributions.

At NNLO (results shown by the red solid lines), using the subtractive renormalization we found sizable improvement for the 3D_3 phase shifts and ϵ_2 . On the other hand, the good agreement with the data observed at LO and NLO is notably worsened for the 1D_2 and 3D_2 partial waves for energies $E_{\text{lab}} > 100$ MeV. In comparison with the non-relativistic NNLO results (shown by the dotted lines), which are exploding beyond $E_{\text{lab}} > 50$ MeV for all D waves, the improvement delivered by our approach is visible, particularly for the 3D_3 partial wave. As noticed in Ref. [62], strong disagreement with the empirical data is caused by unphysical short-distance components of the non-relativistic TPE potential. Following the suggestion of that work to use an alternative regularization scheme instead of the dimensional regularization, we apply the cutoff regularization with the cutoff Λ varying from 500 MeV to 800 MeV to loop integrals in TPE diagrams. The corresponding NLO and NNLO results for phase shifts are presented as the light-blue and red

bands in Fig. 5. For the total angular momentum $j = 2$, i.e. in 1D_2 and 3D_2 partial waves, the improvement is visible. For the 3D_3 phase shift and the ϵ_2 mixing angle the results are similar to the previous ones using the subtractive renormalization in the limit of a removed regulator. This observation is in line with our expectations since the calculated TPE potential has a milder ultraviolet behavior and the short-distance contribution of loop integrals is suppressed in comparison with the non-relativistic case. Note that we do not show the 3D_1 phase shift due to the strong coupling between the 3D_1 and 3S_1 channels.

2. F -waves

Differently from the case of the D -waves, the empirical phase shifts for F -waves are quite small (less than 5°). Our results for the F -wave phase shifts and mixing angle ϵ_3 are shown in Fig. 6. The LO results for 1F_3 , 3F_2 , 3F_3 and ϵ_3 roughly match the data, while the OPE contribution for 3F_4 is very small. The inclusion of the NLO terms leads mainly to small corrections, however visible improvement is seen in the 3F_2 partial wave. Up to NNLO our results for the 1F_3 , 3F_3 , and 3F_4 partial waves are in a good agreement with the data up to $E_{\text{lab}} = 150$ MeV. For larger energies, the NNLO correction becomes too strong due to the subleading TPE potential. Similar behavior is also observed for the non-relativistic NNLO results. In the 3F_2 partial wave, the correct tendency achieved at NLO is altered by including the subleading TPE potential. Furthermore, we also present

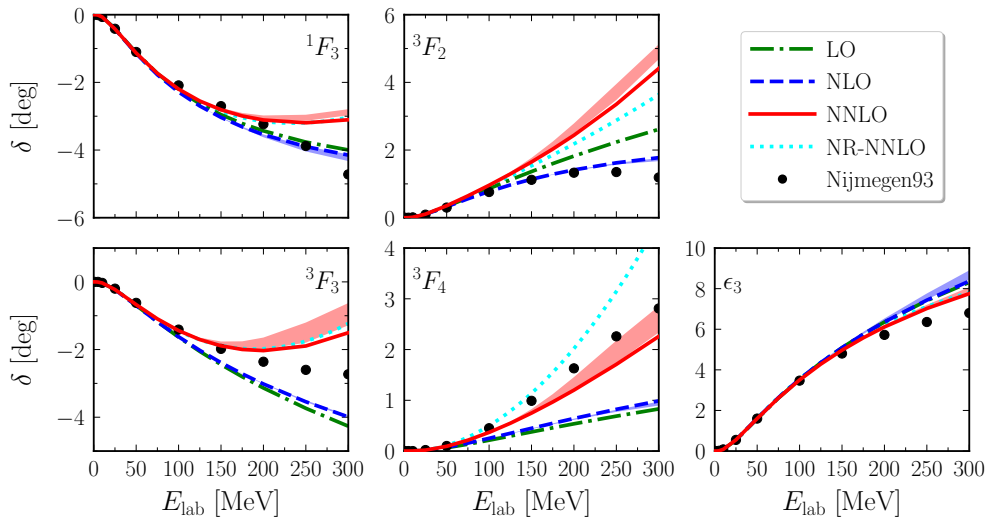


Figure 6. F -wave neutron-proton phase shifts and the mixing angle ϵ_3 for laboratory energies below 300 MeV. Notations are as in Fig. 5.

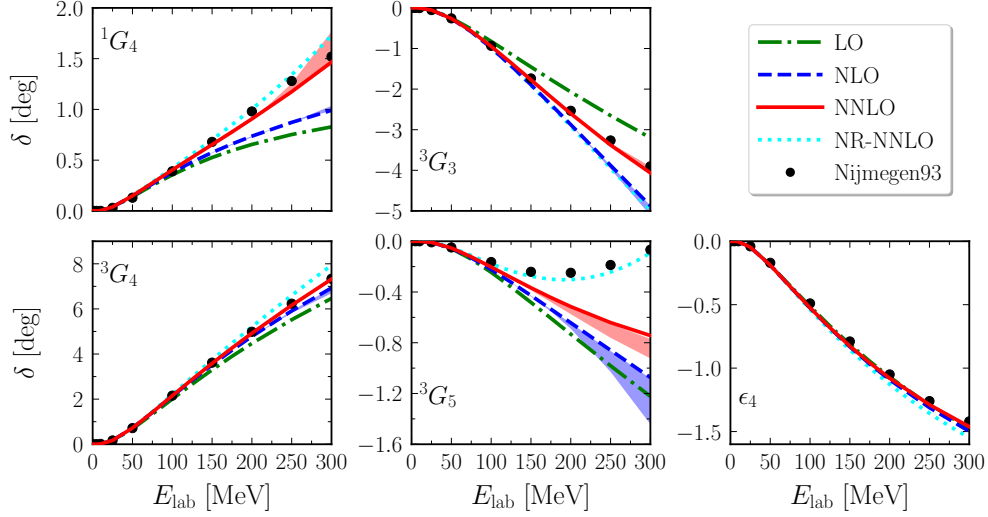


Figure 7. G -wave neutron-proton phase shifts and the mixing angle ϵ_4 for laboratory energies below 300 MeV. Notations are as in Fig. 5.

the NLO and NNLO results with the cutoff regularization of the loop integrals in the TPE potential. They are similar to the results of using the subtractive renormalization with removed regulator limit. This indicates that the short-distance components in the TPE are rather small in our NNLO results for F -waves. Last but not least, we emphasize that the remaining discrepancies between the calculated and empirical F -wave phase shifts are comparable with the natural-size contributions of the leading contact interactions, which appear at sixth order in the EFT expansion [63, 64].

3. G -waves

The G -wave phase shifts and the mixing angle ϵ_4 up to NNLO are shown in Fig. 7. Our NNLO results describe the Nijmegen partial wave analysis rather well, except for the 3G_5 partial wave. The convergence pattern of the chiral expansion for the 3G_3 , 3G_4 partial waves and for ϵ_4 looks very reasonable with the LO potential giving the dominant contribution and the corrections due to the TPE potential being quite small. As for the 1G_4 phase shifts, the NNLO correction of the TPE potential provides a sizable contribution leading to a good agreement with data. In comparison with the NNLO results of non-relativistic ChEFT, our approach gives a slightly better description for 1G_4 , 3G_3 , 3G_4 partial waves and for ϵ_4 .

The situation is different for the 3G_5 partial wave, where the non-relativistic result shows a rather good agreement with the data at NNLO. This agreement is, however, accidental. In particular,

the relativistic corrections to the TPE potential $\propto c_i/m_N$, which in the non-relativistic counting scheme appear at fifth chiral order (i.e., at $N^4\text{LO}$), are of the same size as the difference between the NNLO and NR-NNLO lines in Fig. 7, see Ref. [65]. These contributions are already taken into account in our NNLO results along with an infinite set of c_i/m_N^n , $n \geq 2$, corrections. Thus, we expect the convergence of the covariant chiral EFT approach for this partial wave to be superior as compared to the non-relativistic framework. It is also worth emphasizing that the empirical phase shifts in the 3G_5 channel reflect a subtle interplay between a repulsive long-range and attractive short-range interactions and appear to be much smaller than those in other G -waves. It is, therefore, not straightforward to draw conclusions about the convergence of the chiral expansion in this particular partial wave. We also note in this context that the small NLO correction we found in this channel is due to a cancelation between the individually larger contributions of the leading TPE potential and the once-iterated OPE potential.

For G -waves, the results with the cutoff regularization of the loop integrals in the TPE potential are similar to those using the subtractive renormalization with removed regulator limit.

4. H -waves

In Fig. 8 we present the H -wave phase shifts and the mixing angle ϵ_5 . Basically, the OPE potential can achieve a rather good description of Nijmegen data, except for the 3H_6 partial wave. The corrections due to the TPE are quite small. For the 3H_5 and 3H_6 phase shifts, the subleading TPE potential is needed to describe the empirical phase shifts for $E_{\text{lab}} > 150$ MeV. The NNLO results of 3H_6 phase shifts are slightly lower than the empirical data, while the NNLO potential gives very small positive contributions for the 3H_4 phase shifts. However such differences are insignificant due to the small empirical values of the 3H_4 and 3H_6 phase shifts (less than 0.5°). In comparison with the NNLO results of the non-relativistic scheme, a different tendency is seen in the 3H_6 partial wave. The non-relativistic NNLO result overshoots the empirical phase shifts, while our NNLO result lies below the data points. For the other H -waves and the mixing angle ϵ_5 , our approach gives a slightly better description than the non-relativistic formalism.

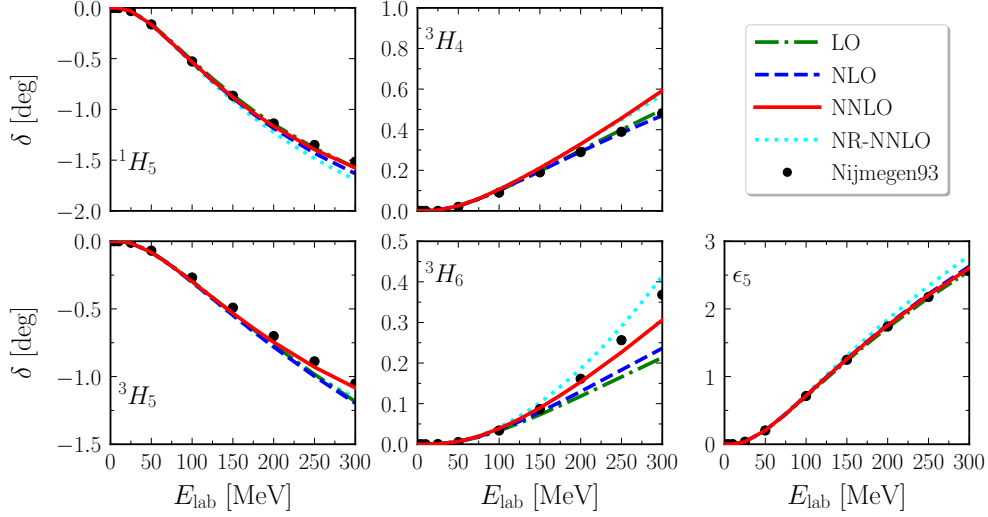


Figure 8. H -wave neutron-proton phase shifts and the mixing angle ϵ_5 for laboratory energies below 300 MeV. Notations are as in Fig. 5.

5. I -waves

The I -wave phase shifts and mixing angle ϵ_6 are shown in Fig. 9, where the pure OPE potential already provides a very good approximation. Although the NLO and NNLO corrections are relatively small, their contributions are visible and slightly improve the description of Nijmegen data with $E_{\text{lab}} > 200$ MeV, particularly for the 1I_6 , 3I_5 , and 3I_7 partial waves. Furthermore, our NNLO result is globally similar to the one of the non-relativistic approach.

IV. SUMMARY AND PERSPECTIVE

In this paper we have worked out the nucleon-nucleon interaction up to NNLO in the framework of manifestly Lorentz-invariant ChEFT. We have renormalized the one-loop diagrams contributing to the TPE potential and the scattering amplitude by using the subtractive renormalization. In the large nucleon mass limit, the resulting TPE potential is consistent with its non-relativistic counterpart. Using the one-loop order approximation we calculated the NN phase shifts and mixing angles for partial waves with the orbital angular momentum $l \geq 2$ and compared the obtained results with the corresponding ones of the non-relativistic formulation. We found that the description of D waves, particularly for 3D_3 , is improved because of the relatively small contribution of TPE diagrams. For the other peripheral partial waves, both approaches give (globally) similar results.

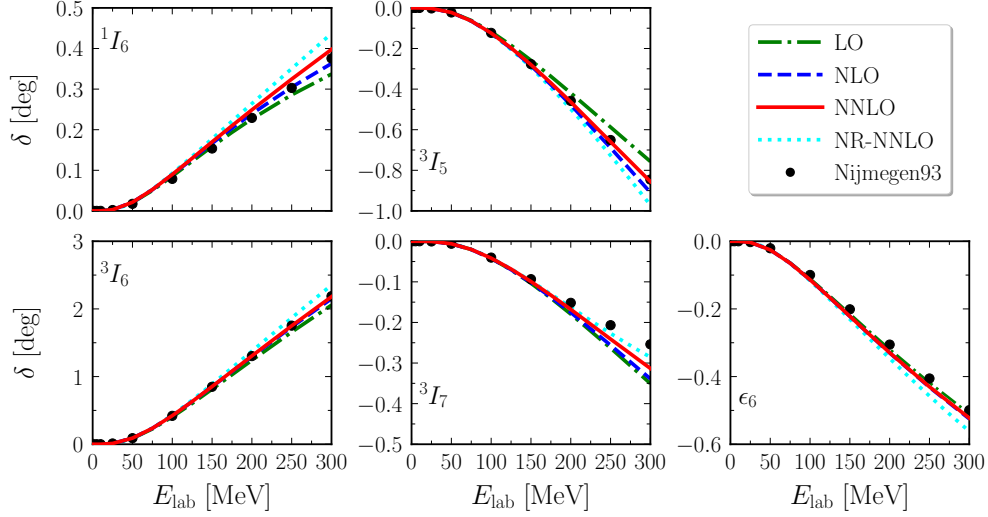


Figure 9. I -wave neutron-proton phase shifts and the mixing angle ϵ_6 for laboratory energies below 300 MeV. Notations are as in Fig. 5.

For the 3G_5 partial wave, our results indicate a better convergence beyond NNLO compared to the non-relativistic approach.

Besides the higher partial waves, the description of the S and P partial waves and the deuteron bound state is most relevant in formulating the realistic NN force. Two strategies are available for considering the S and P partial waves at NNLO: 1) Restrict the non-perturbative treatment to our non-singular LO potential and include the NLO and NNLO corrections perturbatively. This would allow to systematically remove all divergences from the amplitude; 2) Treat the full NNLO potential non-perturbatively to obtain the NN scattering amplitude by solving the Kadyshevsky equation. The milder UV behavior of the effective potential and the scattering equation provide with a larger range of admissible cutoff-values, which is a welcome feature for the few/many-body calculations.² Work along these lines is in progress.

ACKNOWLEDGMENTS

This work was supported in part by BMBF (Grant No. 05P18PCFP1), by DFG and NSFC through funds provided to the Sino-German CRC 110 “Symmetries and the Emergence of Structure in QCD” (NSFC Grant No. 11621131001, DFG Project-ID 196253076 - TRR 110), by DFG through the CRC 1044 “The Low-Energy Frontier of the Standard Model” (Project ID 204404729

² Both strategies are of course also applicable for peripheral phases.

- SFB 1044), by the Cluster of Excellence “Precision Physics, Fundamental Interactions, and Structure of Matter” (PRISMA⁺, EXC 2118/1) within the German Excellence Strategy (Project ID 39083149), by the Georgian Shota Rustaveli National Science Foundation (Grant No. FR17-354), by ERC AdG NuclearTheory (Grant No. 885150) and by the EU Horizon 2020 research and innovation programme (STRONG-2020, grant agreement No. 824093).

- [1] S. Weinberg, *Physica A* **96**, 327-340 (1979).
- [2] S. Weinberg, *Phys. Lett. B* **251**, 288-292 (1990).
- [3] S. Weinberg, *Nucl. Phys. B* **363**, 3-18 (1991).
- [4] P. F. Bedaque, U. van Kolck, *Ann. Rev. Nucl. Part. Sci.* **52**, 339 (2002), [[arXiv:nucl-th/0203055](#)].
- [5] E. Epelbaum, *Prog. Part. Nucl. Phys.* **57**, 654 (2006), [[arXiv:nucl-th/0509032](#)].
- [6] E. Epelbaum, H. W. Hammer and U.-G. Meißner, *Rev. Mod. Phys.* **81**, 1773 (2009), [[arXiv:0811.1338](#) [nucl-th]].
- [7] R. Machleidt and D. R. Entem, *Phys. Rept.* **503**, 1 (2011), [[arXiv:1105.2919](#) [nucl-th]].
- [8] E. Epelbaum and U.-G. Meißner, *Ann. Rev. Nucl. Part. Sci.* **62**, 159 (2012), [[arXiv:1201.2136](#) [nucl-th]].
- [9] D. B. Kaplan, M. J. Savage and M. B. Wise, *Nucl. Phys. B* **478**, 629-659 (1996), [[arXiv:nucl-th/9605002](#) [nucl-th]].
- [10] S. R. Beane, T. D. Cohen and D. R. Phillips, *Nucl. Phys. A* **632**, 445-469 (1998), [[arXiv:nucl-th/9709062](#) [nucl-th]].
- [11] D. B. Kaplan, M. J. Savage and M. B. Wise, *Phys. Lett. B* **424**, 390-396 (1998), [[arXiv:nucl-th/9801034](#) [nucl-th]].
- [12] M. C. Birse, J. A. McGovern and K. G. Richardson, *Phys. Lett. B* **464**, 169-176 (1999), [[arXiv:hep-ph/9807302](#) [hep-ph]].
- [13] A. Nogga, R. G. E. Timmermans and U. van Kolck, *Phys. Rev. C* **72**, 054006 (2005), [[arXiv:nucl-th/0506005](#) [nucl-th]].
- [14] B. Long and U. van Kolck, *Annals Phys.* **323**, 1304-1323 (2008), [[arXiv:0707.4325](#) [quant-ph]].
- [15] M. C. Birse, *PoS CD09*, 078 (2009), [[arXiv:0909.4641](#) [nucl-th]].
- [16] K. Harada, H. Kubo and Y. Yamamoto, *Phys. Rev. C* **83**, 034002 (2011), [[arXiv:1012.2716](#) [nucl-th]].
- [17] B. Long and C. J. Yang, *Phys. Rev. C* **84**, 057001 (2011), [[arXiv:1108.0985](#) [nucl-th]].
- [18] B. Long and C. J. Yang, *Phys. Rev. C* **85**, 034002 (2012), [[arXiv:1111.3993](#) [nucl-th]].

- [19] K. Harada, H. Kubo, T. Sakaeda and Y. Yamamoto, [arXiv:1311.3063](#) [nucl-th].
- [20] E. Epelbaum and J. Gegelia, Eur. Phys. J. A **41**, 341-354 (2009), [[arXiv:0906.3822](#) [nucl-th]].
- [21] E. Epelbaum, J. Gegelia and U.-G. Meißner, Nucl. Phys. B **925**, 161-185 (2017), [[arXiv:1705.02524](#) [nucl-th]].
- [22] E. Epelbaum, A. M. Gasparyan, J. Gegelia, U.-G. Meißner and X.-L. Ren, Eur. Phys. J. A **56**, 152 (2020), [[arXiv:2001.07040](#) [nucl-th]].
- [23] E. Epelbaum, J. Gegelia, H. P. Huesmann, U.-G. Meißner and X.-L. Ren, Few Body Syst. **62**, 51 (2021), [[arXiv:2104.01823](#) [nucl-th]].
- [24] M. P. Valderrama, Int. J. Mod. Phys. E **25**, 1641007 (2016), [[arXiv:1604.01332](#) [nucl-th]].
- [25] J. Gegelia and S. Scherer, Int. J. Mod. Phys. A **21**, 1079 (2006), [[arXiv:nucl-th/0403052](#)].
- [26] E. Epelbaum and U.-G. Meißner, Few Body Syst. **54**, 2175 (2013), [[nucl-th/0609037](#)].
- [27] E. Epelbaum, A. M. Gasparyan, J. Gegelia and U.-G. Meißner, Eur. Phys. J. A **54**, 186 (2018), [[arXiv:1810.02646](#) [nucl-th]].
- [28] H.-W. Hammer, S. König and U. van Kolck, Rev. Mod. Phys. **92**, 025004 (2020), [[arXiv:1906.12122](#) [nucl-th]].
- [29] U. van Kolck, Front. in Phys. **8**, 79 (2020), [[arXiv:2003.06721](#) [nucl-th]].
- [30] A. M. Gasparyan and E. Epelbaum, [[arXiv:2110.15302](#) [nucl-th]].
- [31] G. P. Lepage, [arXiv:nucl-th/9706029](#).
- [32] J. Gegelia, J. Phys. G **25**, 1681 (1999).
- [33] T. S. Park, K. Kubodera, D. P. Min, and M. Rho, Nucl. Phys. A **646**, 83 (1999), [[arXiv:nucl-th/9807054](#)].
- [34] G. P. Lepage, *Conference summary*, Prepared for INT Workshop on Nuclear Physics with EFT, Seattle, Washington, 25-26 Feb 1999.
- [35] E. Epelbaum, W. Glöckle, U.-G. Meißner, Nucl. Phys. A **747**, 362 (2005), [[arXiv:nucl-th/0405048](#)].
- [36] T. Frederico, V. S. Timoteo and L. Tomio, Nucl. Phys. A **653**, 209-221 (1999), [[arXiv:nucl-th/9902052](#) [nucl-th]].
- [37] V. S. Timoteo, T. Frederico, A. Delfino and L. Tomio, Phys. Lett. B **621**, 109-118 (2005), [[arXiv:nucl-th/0508006](#) [nucl-th]].
- [38] C. J. Yang, C. Elster and D. R. Phillips, Phys. Rev. C **77**, 014002 (2008), [[arXiv:0706.1242](#) [nucl-th]].
- [39] C. J. Yang, C. Elster and D. R. Phillips, Phys. Rev. C **80**, 034002 (2009), [[arXiv:0901.2663](#) [nucl-th]].
- [40] S. R. Beane and R. C. Farrell, [[arXiv:2112.05800](#) [nucl-th]].

- [41] I. Tews, Z. Davoudi, A. Ekström, J. D. Holt, K. Becker, R. Briceño, D. J. Dean, W. Detmold, C. Drischler and T. Duguet, *et al.*, [[arXiv:2202.01105](#) [nucl-th]].
- [42] E. Epelbaum and J. Gegelia, Phys. Lett. B **716**, 338 (2012), [[arXiv:1207.2420](#) [nucl-th]].
- [43] V. Baru, E. Epelbaum, J. Gegelia and X.-L. Ren, Phys. Lett. B **798**, 134987 (2019), [[arXiv:1905.02116](#) [nucl-th]].
- [44] V. G. Kadyshevsky, Nucl. Phys. B **6**, 125 (1968).
- [45] R. Higa and M. R. Robilotta, Phys. Rev. C **68**, 024004 (2003), [[arXiv:nucl-th/0304025](#) [nucl-th]].
- [46] R. Higa, M. R. Robilotta and C. A. da Rocha, Phys. Rev. C **69**, 034009 (2004), [[arXiv:nucl-th/0310011](#) [nucl-th]].
- [47] X.-L. Ren, K. W. Li, L. S. Geng, B. W. Long, P. Ring and J. Meng, Chin. Phys. C **42**, 014103 (2018), [[arXiv:1611.08475](#) [nucl-th]].
- [48] Y. Xiao, C. X. Wang, J. X. Lu and L. S. Geng, Phys. Rev. C **102**, 054001 (2020), [[arXiv:2007.13675](#) [nucl-th]].
- [49] C. X. Wang, J. X. Lu, Y. Xiao and L. S. Geng, Phys. Rev. C **105**, 014003 (2022), [[arXiv:2110.05278](#) [nucl-th]].
- [50] J. X. Lu, C. X. Wang, Y. Xiao, L. S. Geng, J. Meng and P. Ring, [[arXiv:2111.07766](#) [nucl-th]].
- [51] J. Gasser and H. Leutwyler, Ann. Phys. (N.Y.) **158**, 142 (1984).
- [52] S. Bellucci, J. Gasser and M. E. Sainio, Nucl. Phys. B **423**, 80-122 (1994) [erratum: Nucl. Phys. B **431**, 413-414 (1994)], [[arXiv:hep-ph/9401206](#) [hep-ph]].
- [53] J. Gasser, M. E. Sainio and A. Svarc, Nucl. Phys. B **307**, 779-853 (1988).
- [54] N. Fettes, U.-G. Meißner, M. Mojzis and S. Steininger, Annals Phys. **283**, 273-302 (2000) [erratum: Annals Phys. **288**, 249-250 (2001)], [[arXiv:hep-ph/0001308](#) [hep-ph]].
- [55] E. Epelbaum, Eur. Phys. J. A **34**, 197-214 (2007), [[arXiv:0710.4250](#) [nucl-th]].
- [56] N. Kaiser, R. Brockmann and W. Weise, Nucl. Phys. A **625**, 758-788 (1997), [[arXiv:nucl-th/9706045](#) [nucl-th]].
- [57] K. Erkelenz, R. Alzetta and K. Holinde, Nucl. Phys. A **176**, 413-432 (1971).
- [58] J. Gasser and U.-G. Meißner, Phys. Lett. B **258**, 219-224 (1991).
- [59] M. Hoferichter, J. Ruiz de Elvira, B. Kubis and U.-G. Meißner, Phys. Rept. **625**, 1-88 (2016), [[arXiv:1510.06039](#) [hep-ph]].
- [60] D. Siemens, J. Ruiz de Elvira, E. Epelbaum, M. Hoferichter, H. Krebs, B. Kubis and U.-G. Meißner, Phys. Lett. B **770**, 27-34 (2017), [[arXiv:1610.08978](#) [nucl-th]].

- [61] V. G. J. Stoks, R. A. M. Klomp, M. C. M. Rentmeester and J. J. de Swart, Phys. Rev. C **48**, 792-815 (1993).
- [62] E. Epelbaum, W. Gloeckle and U.-G. Meißner, Eur. Phys. J. A **19**, 125-137 (2004), [[arXiv:nucl-th/0304037](#) [nucl-th]].
- [63] P. Reinert, H. Krebs and E. Epelbaum, Eur. Phys. J. A **54**, 86 (2018), [[arXiv:1711.08821](#) [nucl-th]].
- [64] E. Epelbaum, H. Krebs and P. Reinert, Front. in Phys. **8**, 98 (2020), [[arXiv:1911.11875](#) [nucl-th]].
- [65] D. R. Entem, N. Kaiser, R. Machleidt and Y. Nosyk, Phys. Rev. C **91**, 014002 (2015), [[arXiv:1411.5335](#) [nucl-th]].